

Optical and EPR study of the nickel two-electron-trap state in GaP

U. Kaufmann, W. H. Koschel, and J. Schneider

Institut für Angewandte Festkörperphysik der Fraunhofer-Gesellschaft,

D-7800 Freiburg, Eckerstrasse 4

J. Weber

Universität Stuttgart, 4. Physikalisches Institut, D-7000 Stuttgart, Pfaffenwaldring 57

(Received 17 November 1978)

The infrared luminescence and the absorption spectra of the nickel two-electron-trap state, $\text{Ni}^+ 3d^9$, have been observed and analyzed in GaP. The spectra do not exhibit full mirror symmetry relative to the common zero-phonon line (ZPL) at 5354 cm^{-1} . Chemical identification of the defect is based on the fine structure of the ZPL which is shown to arise from an isotope effect. The Zeeman splitting of the ZPL in fields up to 5.3 T unambiguously demonstrates that the zero-phonon transition occurs between a cubic Γ_8 excited and a Γ_7 ground state, implying that the center is in the $\text{Ni}^+ 3d^9$ charge state. The analysis of the Zeeman data yields $g = -0.94$ for the Γ_7 state and $g_1 = 1.45$, $qg_2 = -0.23$ for the Γ_8 -state g factors. The Ni^+ center was also identified in the EPR spectrum of GaP:Ni and the EPR g value is fully consistent with the Zeeman results. Certain details of the optical spectra and the strongly quenched g factors indicate a moderate Jahn-Teller (JT) coupling within the 2T_2 , and also a moderate JT coupling within the 2E state of Ni^+ . It is shown that static-crystal-field theory is insufficient to account for the data, and a consistent interpretation based on existing JT theories is presented.

I. INTRODUCTION

Transition-metal ions of the $3d$ series are almost inevitable contaminations of most semiconductors. It is known that these impurities form deep states within the energy gap. One reason for the current interest in such centers in III-V compounds is their often negative influence on the semiconducting and optoelectronic properties of device-grade material.

Early electrical measurements indicated that $3d$ ions act as deep acceptors in III-V semiconductors.¹ However, only recent electron-paramagnetic-resonance (EPR) studies²⁻⁵ have revealed that certain $3d$ ions are not simple acceptors but can also trap two electrons in n -type material. In this work optical and EPR results are presented which demonstrate that nickel is such a two-electron trap in n -type GaP. The necessity for a thorough characterization of Ni in GaP stems from the fact that Ni has been reported⁶ to be a persistent, inadvertent contaminant even in device-grade GaP.

Hall measurements⁷ have shown that the neutral Ni acceptor, $\text{Ni}^{3+} 3d^7$, has a hole activation energy of $\sim 0.5 \text{ eV}$. In contrast to the neutral acceptor state,⁸ the singly ionized acceptor state, $\text{Ni}^{2+} 3d^8$, is not EPR detectable, because of its diamagnetic ground state A_1 . However, the Ni^{2+} charge state is easily observable in optical absorption since it induces a characteristic $3d$ - $3d$ absorption band centered at $0.97 \mu\text{m}$.⁹ The doubly ionized Ni acceptor state, $\text{Ni}^+ 3d^9$, is

again detectable by EPR. The $3d$ - $3d$ ir absorption and emission spectrum, the Zeeman splitting of its zero-phonon line (ZPL), and the EPR spectrum of this charge state are analyzed in detail in this paper. Chemical identification of the Ni^+ center is based on an isotope structure of the ZPL. The Zeeman splitting of the ZPL confirms its assignment to Ni^+ . Further, the optical Zeeman spectra are shown to be fully consistent with the EPR data of Ni^+ . The experimental results are interpreted in the framework of crystal-field theory extended to include covalency effects and vibronic coupling. It will be seen that the Ni^+ center in GaP exhibits a moderate vibronic coupling with asymmetric vibrational modes in both its ground and excited state.

Optical $3d$ - $3d$ spectra of divalent transition-metal centers have been studied extensively, especially in II-VI compounds.¹⁰ On the other hand, optical data about monovalent transition-metal impurities are very sparse. To our knowledge, so far, only one example has been reported in the literature. This is the Ni^+ center in the chalcopyrite hosts CuAlS_2 , CuGaS_2 , and AgGaS_2 .¹¹

II. EXPERIMENTAL

The luminescence spectra were measured with 0.75- and 1.0-m grating monochromators using a

cooled PbS cell for detection. The samples were immersed in liquid helium either at 4.2 K or below the λ point. Luminescence was excited with an argon-ion laser. The maximum available power incident on the sample was ~ 1 W. For Zeeman studies, a superconducting solenoid covering a field range up to 5.3 T was used.

Absorption measurements were performed with a 0.75-m grating monochromator equipped with a double-beam accessory described elsewhere.¹² Samples were mounted on the cold finger of a liquid-helium Joule-Thompson cooler. An uncooled PbS cell was used for light detection. To reduce water-vapor absorption in the near ir, the optical path was purged with dry air.

EPR spectra were taken at 9.5 GHz with the sample mounted on the cold finger of a continuous-flow liquid-He cryostat allowing temperature regulation between 4.2 and 300 K. Since the temperature was not measured directly at the sample, the actual sample temperatures might be slightly higher than the nominal values quoted in Sec. IV C.

The starting material used for sample preparation was liquid-encapsulation Czochralski-grown *n*-type (Te doped, 1.5×10^{17} cm⁻³) and semi-insulating (Cr doped, 10^{16} cm⁻³) GaP. Thin layers of Ni were evaporated onto the crystal surfaces. Subsequently the samples were heated to temperatures between 1000° and 1200°C in closed quartz ampoules for periods of one to two days. Some luminescence spectra were also obtained from as-grown, device-grade, vapor-phase GaP:Te:N epitaxial layers.

III. THEORY

A. Energy-level scheme for $3d^9$ in T_d

The free Ni^{2+} ion has the electron configuration $3d^9$, which leads to a single LS term 2D . Under the action of a tetrahedral crystal field, V_{cub} (splitting $\Delta = 10Dq$), and spin-orbit interaction (λ_1, λ_2), this state is split as shown in Fig. 1.^{13,14} The spin-orbit constants λ_1 and λ_2 refer to matrix elements within 2T_2 and between 2T_2 and 2E , respectively. Covalency effects are taken into account by introducing reduction factors k_1 and k_2 to account for the partial quenching of angular momentum through admixture of ligand orbitals in the $3d$ orbitals. When an external magnetic field is applied to the system, the complete Hamiltonian in the static crystal-field approximation can be written

$$\mathcal{H} = V_{cub} + \lambda_{1,2} \vec{L} \cdot \vec{S} + \mu_B \vec{H} \cdot (k_{1,2} \vec{L} + g_e \vec{S}), \quad (1)$$

where $g_e = 2.0023$ is the free-electron spin g factor. The tetrahedral potential V_{cub} contains the usual

third- and fourth-order terms.¹⁵ At low temperatures and in zero magnetic field there is a single $E1$ -allowed transition in absorption ($\Gamma_7 \rightarrow \Gamma_8^{(1)}$), while one expects two $E1$ -allowed transitions in emission ($\Gamma_8^{(1)} \rightarrow \Gamma_7$ and $\Gamma_8^{(1)} \rightarrow \Gamma_8^{(2)}$).

B. g factors

1. The Γ_7 ground state

In the framework of static crystal-field theory, the isotropic g value for the Γ_7 ground state of a $3d^9$ ion is given by¹⁵

$$g_7 = -\frac{1}{3}(g_e + 4k_1). \quad (2)$$

It is well documented that the above relation is insufficient to account for the measured g values of several tetrahedrally coordinated $3d^9$ systems.¹⁶⁻²⁰ This failure was attributed¹⁷⁻²¹ to the influence of a dynamic Jahn-Teller (JT) effect, i.e., the vibrational-electronic (vibronic) coupling of an orbitally degenerate state with asymmetric vibrational modes.²² Ham^{23,24} has shown that this coupling may substantially quench the orbital angular momentum within the vibronic ground state derived from an electronic E or T state, and may therefore reduce the orbital contribution to the g factor and the spin-orbit constant from the values predicted by static crystal-field theory. On the basis of Ham's theory, Clerjaud and Gelineau²¹ have derived an expression for g_7 when the 2T_2 state couples with a single E -type vibrational mode. They found

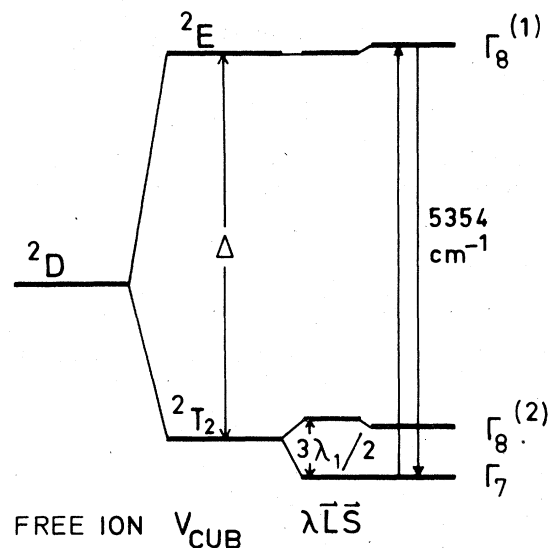


FIG. 1. Energy levels of $Ni^{2+} 3d^9$ in a tetrahedral crystal field.

$$-g_7 = \frac{1}{3} \left[g_e + 4k_1 \left(e^{-3S/2} - \frac{\lambda_1}{\hbar\omega} e^{-3S} [G(3S) + G(\frac{3}{2}S)] \right) + 8 \frac{k_2\lambda_2}{\Delta} (1 - e^{-3S/2}) \right], \quad (3)$$

where $S = E_{JT}/\hbar\omega$ is a measure for the strength of the vibronic coupling, and E_{JT} is the stabilization of the vibronic ground state through coupling with an E mode of energy $\hbar\omega$. In the present work there was no need to include T_2 mode coupling in explaining the data involving the 2T_2 state. For a number of T -state systems subject to JT coupling, e.g., ZnS:Cr²⁺,^{25,26} ZnS:Fe²⁺,²⁷ Mn²⁺ in ZnS, ZnSe, and GaP,²⁸⁻³⁰ and ZnS:Cu²⁺,²¹ the data were satisfactorily explained, neglecting T_2 mode coupling, and in some of these examples this is also justified by direct experimental evidence.^{26,28}

2. The $\Gamma_8^{(1)}$ excited state

Bleaney,³¹ as well as Koster and Statz,³² has shown that the most general spin Hamiltonian linear in the magnetic field, for a cubic Γ_8 state has the form

$$\mathcal{H} = g_1\mu_B\vec{J}\cdot\vec{H} + g_2\mu_B(J_x^3H_x + J_y^3H_y + J_z^3H_z), \quad (4)$$

where $\vec{J} = \vec{L} + \vec{S}$ is the total angular momentum. Since the orbital momentum within a cubic E state vanishes, the above Hamiltonian takes a simpler form for the $\Gamma_8^{(1)}$ of Ni²⁺,²⁴

$$\mathcal{H} = g_1\mu_B\vec{S}\cdot\vec{H} + \frac{1}{2}g_2\mu_B[(3S_zH_z - \vec{S}\cdot\vec{H})U_\theta + 3^{1/2}(S_xH_x - S_yH_y)U_\epsilon], \quad (5)$$

with $S = \frac{1}{2}$. The two-by-two matrices U_θ and U_ϵ act on the basis functions

$$|\theta\rangle \sim 3z^2 - r^2, \quad |\epsilon\rangle \sim 3^{1/2}(x^2 - y^2)$$

of the E state and are defined in Ref. 24. According to crystal-field theory, g_1 and g_2 in Eq. (5) are given by²⁴

$$g_1 = g_e - 4k_2\lambda_2/\Delta, \quad (6a)$$

$$g_2 = -4k_2\lambda_2/\Delta. \quad (6b)$$

Note that Δ has to be taken as negative in Eqs. (6a) and (6b) since these equations refer to an excited 2E state. Therefore λ_2/Δ is positive. Ham²⁴ has also shown that, in the presence of JT coupling, the above Hamiltonian remains valid for the vibronic ground state derived from the electronic $\Gamma_8^{(1)}$ level if g_2 is replaced by

$$g_2' = qg_2, \quad (7)$$

where $\frac{1}{2} \leq q \leq 1$ is a reduction factor which is plot-

ted versus the coupling strength $E_{JT}/\hbar\omega$ in Fig. 2 of Ref. 24.

For some purposes it is convenient to introduce anisotropic g factors $g_8^{(1/2)}$ and $g_8^{(3/2)}$ for the $m = \pm \frac{1}{2}$ and $m = \pm \frac{3}{2}$ substates of $\Gamma_8^{(1)}$, respectively. If \vec{H} is parallel to a $\langle 100 \rangle$ direction they are related to g_1 and g_2 as follows:

$$g_8^{(3/2)} = -(g_1 + qg_2), \quad (8a)$$

$$g_8^{(1/2)} = g_1 - qg_2. \quad (8b)$$

Provided that $qg_2 \ll g_1$, these angular dependent g factors take the form²⁴

$$-g_8^{(3/2)} = g_e - 4 \frac{k_2\lambda_2}{\Delta} - 4q \frac{k_2\lambda_2}{\Delta} f, \quad (9a)$$

$$g_8^{(1/2)} = g_e - 4 \frac{k_2\lambda_2}{\Delta} + 4q \frac{k_2\lambda_2}{\Delta} f, \quad (9b)$$

where

$$f = [1 - 3(l^2m^2 + m^2n^2 + n^2l^2)]^{1/2}, \quad (10)$$

with l, m, n being the direction cosines of \vec{H} , with respect to the cubic axes. For \vec{H} in a $\langle 110 \rangle$ plane we have

$$f = [1 - (\frac{3}{4})\sin^2\theta(1 + 3\cos^2\theta)]^{1/2}, \quad (11)$$

where θ is the angle between \vec{H} and a $\langle 100 \rangle$ direction.

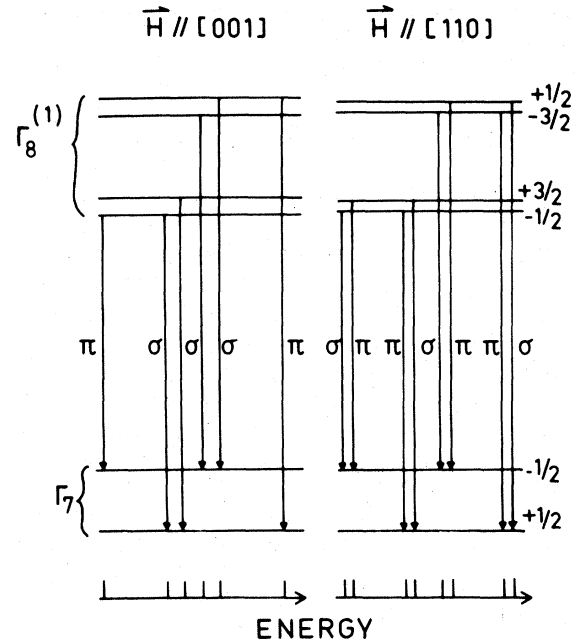


FIG. 2. Splitting of the Γ_7 and $\Gamma_8^{(1)}$ levels of the $3d^9$ configuration in an external magnetic field ($\vec{H} \parallel [001]$ and $\vec{H} \parallel [110]$). Electric dipole allowed transitions are indicated by arrows.

C. Parameters

To evaluate Eqs. (2), (3), and (6), one needs reasonable estimates for the relevant parameters Δ , k_1 , λ_1 , etc. Taking experience from II-VI compounds as guidance,²⁶ we set

$$k_1 = 0.70, \quad k_2 = 0.95, \quad \lambda_1 = 0.8,$$

$$\lambda_0 \approx -480 \text{ cm}^{-1}, \quad \lambda_2 = \lambda_0,$$

where

$$\lambda_0 = -603 \text{ cm}^{-1}$$

is the free-ion spin-orbit coupling constant of Ni^+ . With the Δ value deduced in Sec. IV A, this gives $k_2\lambda_2/\Delta \approx 0.12$.

In calculations involving JT coupling within 2E and 2T_2 , the energy of the effective vibrational mode is assumed to be $\hbar\omega = 350 \text{ cm}^{-1}$ for GaP, a value which is suggested by the comparison with similar system, e.g., $\text{ZnS}:\text{Ni}^+$.²¹ This implies $\lambda_1/\hbar\omega = -1.37$.

The parameter set quoted above will be used for all numerical estimates throughout this paper.

D. Optical transitions in an applied magnetic field

Under the action of an external magnetic field, the Γ_7 and $\Gamma_8^{(1)}$ levels in Fig. 1 are split, as shown in Fig. 2. The multiplicity of $E1$ -allowed transitions is governed by selection rules which are readily obtained with the use of Table I in this paper and Tables X and XXVI of Ref. 13. The labels π and σ

TABLE I. Identification of cubic ${}^2E\Gamma_8m_s$ and ${}^2T_2\Gamma_7m_s$ states with irreducible representations of S_4 and C_s , respectively.

T_d	$S_4 (\bar{H} \parallel \langle 100 \rangle)$	$C_s (\bar{H} \parallel \langle 110 \rangle)$
$\Gamma_8 -\frac{3}{2}$	Γ_7	Γ_4
$\Gamma_8 -\frac{1}{2}$	Γ_6	Γ_4
$\Gamma_8 \frac{1}{2}$	Γ_5	Γ_3
$\Gamma_8 \frac{3}{2}$	Γ_8	Γ_3
$\Gamma_7 -\frac{1}{2}$	Γ_8	Γ_4
$\Gamma_7 \frac{1}{2}$	Γ_7	Γ_3

mean that the electric vector of the radiation is parallel, respectively, perpendicular to the static magnetic field \bar{H} . It should be noted that the identification of the m_s sublevels with specific irreducible representations in Table I differs from that given in Ref. 33. These differences arise from the fact that the Γ_7 and Γ_8 states considered here derive from d -electron states, whereas those considered in Ref. 33 derive from p states. It is obvious from Fig. 2 that the absolute values of all g factors, g_7 , $g_8^{(1/2)}$, and $g_8^{(3/2)}$, can be determined from the experimental Zeeman pattern. The polarization selection rules also fix the relative signs of g_7 , $g_8^{(1/2)}$, and $g_8^{(3/2)}$.

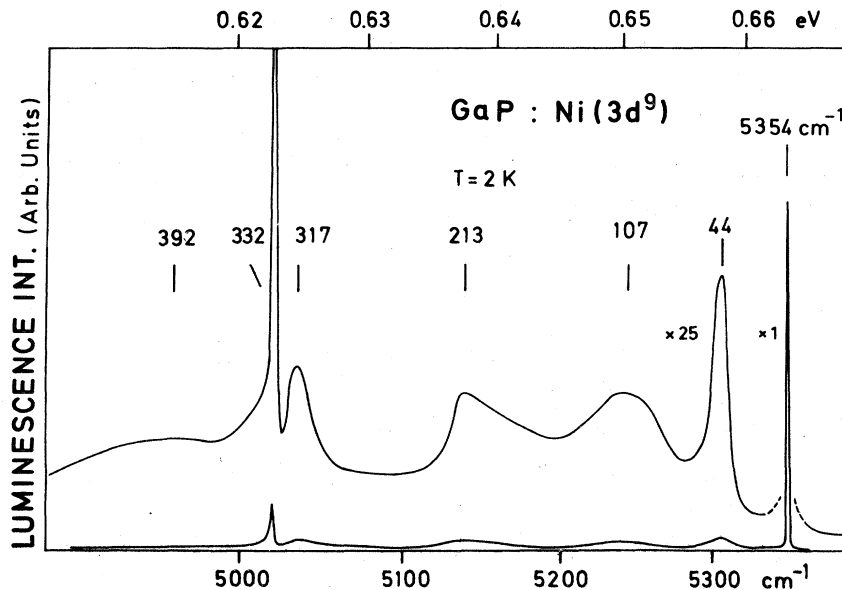


FIG. 3. Photoluminescence spectrum of GaP:Ni at $T = 2 \text{ K}$. The zero-phonon transition is at 5354 cm^{-1} . The energy differences for the phonon sidebands are given in cm^{-1} .

IV. EXPERIMENTAL RESULTS

A. Luminescence and absorption spectra

Figure 3 shows the Ni-induced emission from a Ni-diffused, Te-doped GaP sample.^{34,35} In Sec. V it is shown to arise from an internal $3d-3d$ transition of the isolated Ni^{+3d^9} impurity. Consistent with previous findings of Dean *et al.*,⁶ this spectrum was also observed in nominally pure n -type samples, and even in device-grade Te, N-doped vapor-phase epitaxial layers. The 5354 cm^{-1} ZPL is followed by several phonon replicas, three of which (107, 213, and 392 cm^{-1}) correlate with the energies of the TA (X), LA(L), and LO (Γ) phonons.³⁶ The sharp sideband at 332 cm^{-1} probably involves a totally symmetric local mode analogous to that observed in Mn-doped GaP.^{29,37} Its two-phonon replica appears at 665 cm^{-1} . It is possible that some of the weak sidebands, clearly visible in the corresponding absorption spectrum, were not resolved because of an insufficient signal-to-noise ratio. The origin of the low-energy 44-cm^{-1} line is discussed in Sec. V D.

Figure 4 displays the 5354-cm^{-1} ZPL under high resolution. Its structure is shown, in Sec. V A, to arise from an isotope splitting.

Absorption measurements, performed on Ni-diffused samples, reveal several bands between 2.5 and $0.5\ \mu\text{m}$. In agreement with previous work,^{7,9} a weak unstructured absorption starts near $2.0\ \mu\text{m}$, and

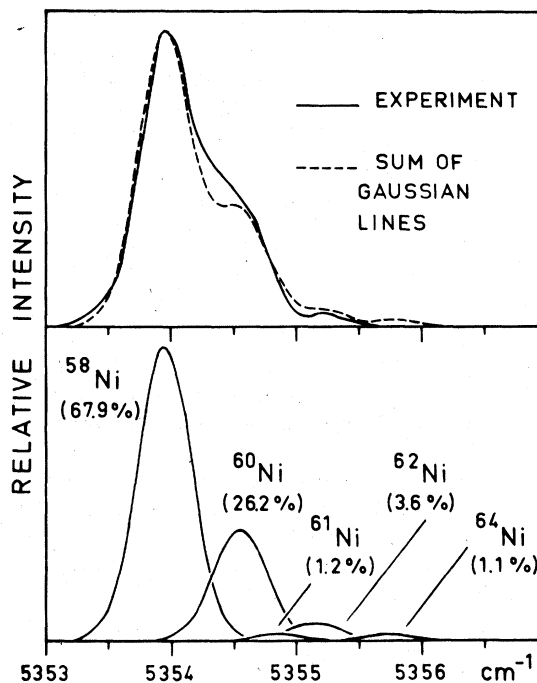


FIG. 4. Structure of the 5354-cm^{-1} ZPL in the photoluminescence spectrum of Fig. 3. The experimental line shape (upper part: solid line) is compared with a theoretical line shape generated by a sum of Gaussian lines as explained in the text.

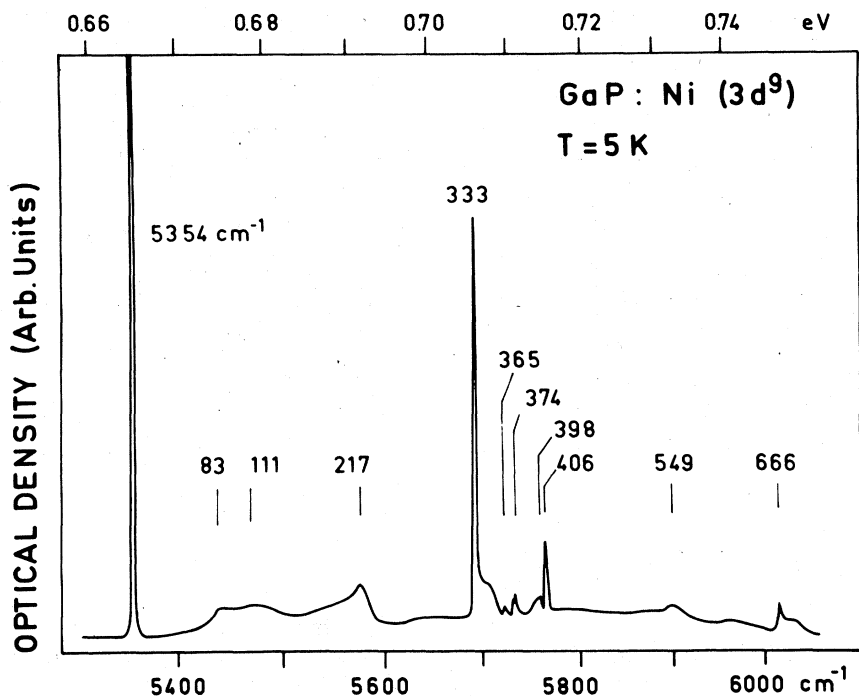


FIG. 5. Absorption spectrum of GaP:Ni at $T = 5\text{ K}$. The zero-phonon transition is again at 5354 cm^{-1} . The energy differences for the phonon side bands are given in cm^{-1} .

a stronger unstructured band has its threshold near $0.85 \mu\text{m}$. A structured band which was formerly⁹ attributed to the ${}^3T_1(F) \rightarrow {}^3T_1(P)$ crystal-field transition of Ni^{2+} is observed at $0.97 \mu\text{m}$. Two new crystal-field bands with ZPL's at 5354 and 4706 cm^{-1} , respectively, were detected. Both bands are only present when Ni is diffused into *n*-type GaP. The longer wavelength absorption possibly arises from the ${}^3T_1(F) \rightarrow {}^3T_2(F)$ transition of Ni^{2+} . The shorter wavelength band is shown in Fig. 5, and its ZPL is seen to coincide with that of the emission in Fig. 3. It is, therefore, attributed to the ${}^2T_2 \rightarrow {}^2E$ crystal-field absorption of Ni^{2+} . The vibronic structure of this absorption is similar to that of the luminescence spectrum. However, the spectra do not display full mir-

ror symmetry relative to the 5354-cm^{-1} ZPL. Note especially that the prominent 44-cm^{-1} sideband seen in emission is absent in absorption. Except for the 333-cm^{-1} local mode, the sideband structure strongly resembles the one-phonon density of states in GaP.³⁶

From the spectra in Figs. 3 and 5, and the level scheme in Fig. 1, one infers that the cubic crystal-field parameter of Ni^{2+} in GaP amounts to $\Delta \approx 10Dq \approx 4800 \text{ cm}^{-1}$.

B. Zeeman splitting of the 5354-cm^{-1} ZPL

The Zeeman splitting of the 5354 cm^{-1} ZPL has been investigated in luminescence in magnetic fields up to 5.3 T . Figure 6 shows the Zeeman pattern obtained in the Voigt configuration ($\vec{k} \perp \vec{H}, \vec{k} \parallel [110], \vec{H} \parallel [001]$). As expected, the corresponding Zeeman pattern obtained in the Faraday configuration ($\vec{k} \parallel \vec{H} \parallel [001]$) was identical with the σ spectrum in Fig. 6. Note that the outermost lines in Fig. 6 display the same shoulder as the zero-

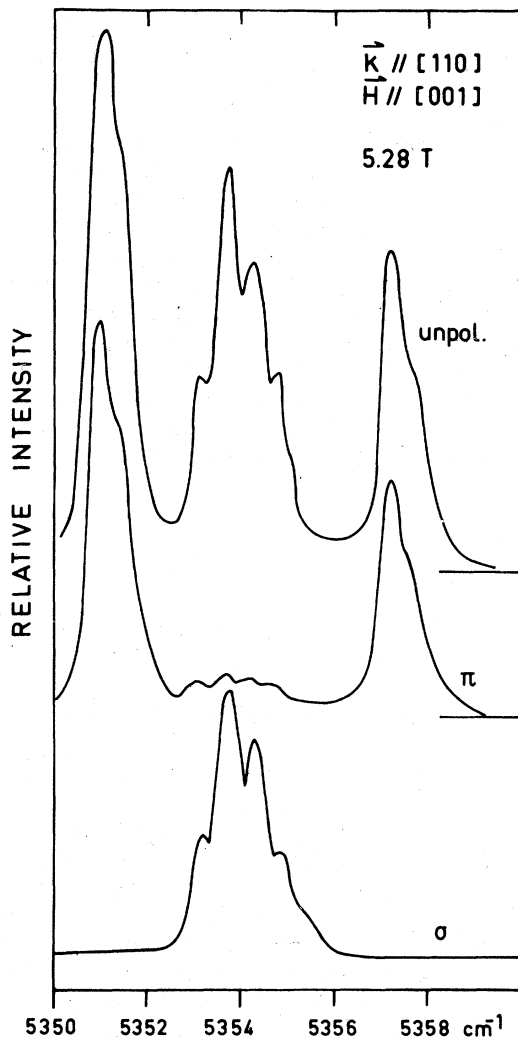


FIG. 6. Zeeman splitting of the 5354-cm^{-1} ZPL in the luminescence spectrum of GaP:Ni at 4 K . (Voigt configuration: $\vec{k} \parallel [110], \vec{H} \parallel [001], 5.28 \text{ T}$.)

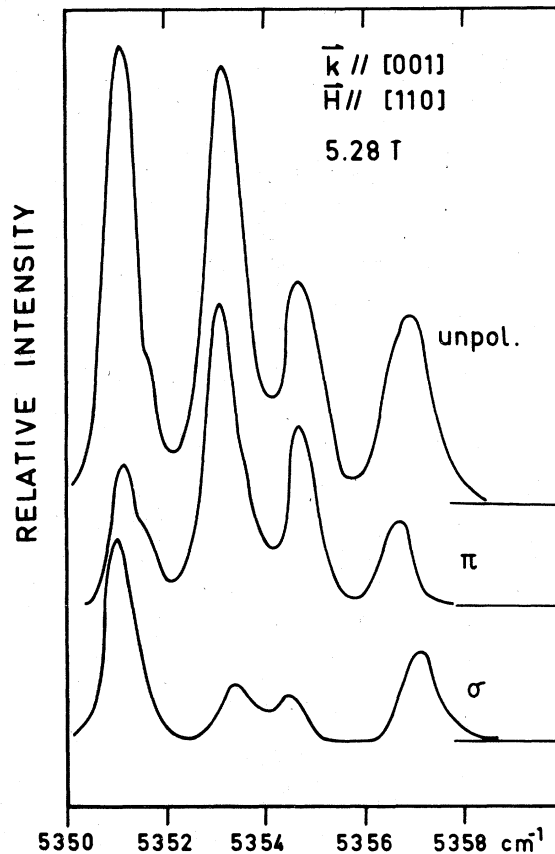


FIG. 7. Zeeman splitting of the 5354-cm^{-1} ZPL in the luminescence spectrum of GaP:Ni at 4 K . (Voigt configuration: $\vec{k} \parallel [001], \vec{H} \parallel [110], 5.28 \text{ T}$.)

field line in Fig. 4, indicating that this structure arises from an isotope effect and not from an unresolved Zeeman splitting. The Voigt spectrum for $\vec{k} \parallel [001]$ and $\vec{H} \parallel [110]$ is shown in Fig. 7.

The peak positions of observed Zeeman lines for the geometry of Fig. 6 are plotted versus H in Fig. 8.

When \vec{H} is rotated in the (110) plane, the individual lines in Figs. 6 and 7 vary in intensity as in position. It has not been possible to measure this angular dependence for all lines, since most of them severely interfere with sharp water-vapor absorption lines. This, together with badly resolved splittings, prevents an accurate recording of line shifts. However, the angular dependence of two lines could be followed over a limited angle range, and this is shown in Fig. 9.

The most accurate g values were determined from the $\vec{H} \parallel [001]$ spectrum as

$$g_7 = -0.94 ,$$

$$g_8^{(1/2)} ([001]) = 1.68 ,$$

$$g_8^{(3/2)} ([001]) = -1.22 ,$$

with an error estimate of 0.06. Together with Eqs. (8a) and (8b) the latter two values imply

$$g_1 = 1.45 ,$$

$$qg_2 = -0.23 .$$

From the polarization characteristics of the Zeeman patterns in Figs. 6 and 7 it follows that the signs of g_7 and $g_8^{(3/2)}$ are opposite to that of $g_8^{(1/2)}$. If g_7 is taken negative according to Eq. (2), g_1 must be positive and g_2 negative, which is consistent with the predictions of Eqs. (6a) and (6b).

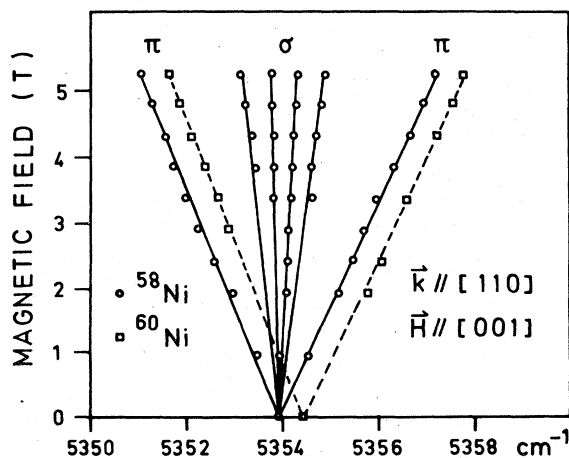


FIG. 8. Peak positions of observed Zeeman lines in GaP:Ni vs magnetic field (Voigt configuration: $\vec{k} \parallel [110], \vec{H} \parallel [001]$).

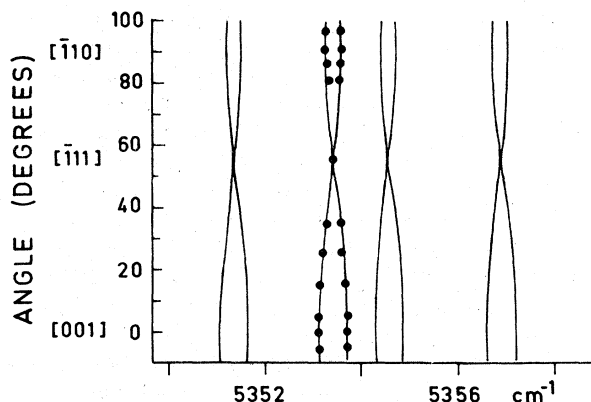


FIG. 9. Peak positions of observed Zeeman lines (points) upon rotating the magnetic field in the (110) plane (5.28 T). The theoretical angular variation, as predicted by Eqs. (9a) and (9b) corresponds to the full lines.

C. EPR

EPR spectra recorded at 4.2 K in the dark revealed a very weak Ni^{3+} signal⁸ and a new isotropic line at $|g| = 0.934$, with a peak-to-peak width of 250 G. This signal is only observed if Ni is diffused into n -type GaP, and it is attributed to an isolated, substitutional Ni^+ impurity. After *in situ* illumination with near-band-gap light (524 nm) we also observed the two-electron-trap state of iron traces ($\text{Fe}^+ 3d^7$)⁴ and the Te-donor line.³⁸ Upon illumination, the Ni^+ EPR intensity was slightly reduced, but this seems to be a thermal rather than an optical effect. The signal vanishes without noticeable broadening above 10 K.

V. DISCUSSION

A. Absorption and luminescence in zero magnetic field

In this section we first show that the optical bands in Figs. 3 and 5 arise from a Ni center, and then demonstrate that it is an isolated Ni^+ impurity with an electron configuration $3d^9$.

The fine structure displayed by the ZPL in Fig. 4 is very likely due to an isotope effect. Such isotope splittings have been reported to occur both in the crystal-field spectra of $\text{ZnO}:\text{Cu}^{2+}$,³⁹ $\text{Al}_2\text{O}_3:\text{Cr}^{3+}$, and $\text{MgO}:\text{Cr}^{3+}$,⁴⁰ and in zero-phonon optical transitions of various traps in semiconductors.⁴¹ We have generated a theoretical line shape by superposition of five Gaussian lines. Their half-widths were inferred from the left part of the measured line shape, and their amplitudes were assumed to be proportional to the natural abundances of ^{58}Ni , ^{60}Ni , ^{61}Ni , ^{62}Ni , and ^{64}Ni . In first order the change, in zero-phonon ener-

gy, scales linearly with the mass differences.⁴⁰ The energy shift per mass unit is then obtained from the experimental trace as 0.3 cm^{-1} . No additional fitting parameter enters the simulated line shape, which is shown as the dashed curve in Fig. 4. The reasonable agreement shows that the structure of the ZPL is of isotopic origin. A final confirmation for this view is provided by the Zeeman splitting in Fig. 8. It demonstrates that the peak (circles, ^{58}Ni) and the shoulder (squares, mainly ^{60}Ni) exhibit an identical magnetic field splitting, as is expected for isotopic satellites.

In principle Ni^{3+} , Ni^{2+} , and Ni^+ can induce crystal-field absorptions in the $2\text{-}\mu\text{m}$ wavelength range. Therefore, it is not possible to decide *a priori* from which Ni charge state the spectra in Figs. 3 and 5 arise. However, the samples were *n* type before Ni diffusion, so it appears unlikely that the spectra are due to Ni^{3+} . In addition, we find that the intensity ratio between the ${}^3T_1(F) \rightarrow {}^3T_1(P)$ Ni^{2+} absorption at $0.97 \mu\text{m}$, and the $1.8\text{-}\mu\text{m}$ band depends markedly on the diffusion temperature. This means that the intensity of the $1.8\text{-}\mu\text{m}$ band is not correlated with the Ni^{2+} concentration as inferred from the $0.97\text{-}\mu\text{m}$ band intensity, and demonstrates that the $1.8\text{-}\mu\text{m}$ band does not result from Ni^{2+} . It is, therefore, reasonable to ascribe this band to Ni^+ , and this assignment is confirmed by the Zeeman data as discussed in Sec. VB.

While there is little doubt that the broad, unstructured absorption starting near $2 \mu\text{m}$, in GaP:Ni arises from a $\text{Ni}^{3+} \rightarrow \text{Ni}^{2+} + h$ transition,⁷ the origin of the $0.85\text{-}\mu\text{m}$ absorption in Ref. 7 is not firmly established. However, preliminary EPR data⁴² indicate that this optical band is correlated with the Ni^{3+} EPR excitation band, thus suggesting that the $0.85\text{-}\mu\text{m}$ threshold is associated with the transition $\text{Ni}^{2+} \rightarrow \text{Ni}^{3+} + e$. So far, it has not been possible to locate an absorption band which might be attributed to a transition $\text{Ni}^{2+} \rightarrow \text{Ni}^+ + h$, nor could we find an excitation or quenching band of the Ni^+ EPR signal. Therefore no information about the ionization energy of the second hole from the Ni center is available.

B. Zeeman splitting of the 5354-cm^{-1} ZPL

The multiplicity of lines and their polarizations in the Zeeman patterns of Figs. 6 and 7 are fully consistent with the expectations for the $\Gamma_8^{(1)} \rightarrow \Gamma_7$ transition of Ni^+ , if g_7 and $g_8^{(3/2)}$ have a sign opposite to that of $g_8^{(1/2)}$. This sign difference is consistent with the predictions of Eqs. 2, (9a), and (9b). The anisotropic nature of the Zeeman splitting expected for a transition involving a cubic Γ_8 level is obvious from the experimental points in Fig. 9. The theoretical angular dependence as predicted by Eqs. (9a) and (9b) fits the data reasonably well. These facts confirm that the 5354-cm^{-1} ZPL in GaP:Ni arises from the $\Gamma_8^{(1)} \rightarrow \Gamma_7$ crystal-field transition of the Ni two-

electron-trap state, Ni^+ . In Ref. 6 the 5354 cm^{-1} ZPL had been assigned to the ${}^3T_2(F) \rightarrow {}^3T_1(F)$ crystal-field transition of Ni^{2+} . This would imply that the 5354-cm^{-1} ZPL is due to a transition from a triplet, T_1 or T_2 , to a singlet A_1 spin-orbit level.⁴³ The present Zeeman results are in conflict with this interpretation.

C. EPR

The identification of the $|g| = 0.934$ EPR signal in GaP:Ni with Ni^+ is based on the following observations: The signal is only observed after diffusion of Ni into *n*-type material. It disappears above 10 K due to strong spin-lattice coupling⁴⁴ consistent with previous EPR results on Ni^+ in ZnS and ZnSe.^{16,17} The g value is incompatible with any other simple Ni center. Finally, and perhaps most convincing, the EPR g_7 value is identical with that obtained from the optical Zeeman spectra for the Γ_7 ground state of Ni^+ . The absolute value of the Ni^+ g_7 factor is close to the value of the isotropic part of the hole g factor in GaP ($g_1 = 1.02$ and $g_1 = 1.25$ for Zn and Cd, respectively⁴⁵). This is believed to be a mere coincidence.

The present EPR and absorption data demonstrate that Ni^{3+} , Ni^{2+} , and Ni^+ are stable charge states in originally *n*-type GaP diffused with Ni. There is also evidence from the absorption spectra that Ni^+ is the dominant charge state as long as the concentration of Ni is small compared with that of the donor dopant. This situation, of course, always prevails for *n*-type GaP undeliberately contaminated with Ni.

D. Jahn-Teller effects in the 2T_2 and 2E states

1. 2T_2 ground state

There are two independent indications that the 2T_2 state exhibits a dynamic JT effect. First, the small g_7 value and second the lack of the 44-cm^{-1} sideband in the absorption spectrum.

To fit g_7 with the static crystal-field expression, Eq. (2), would require a covalency reduction factor $k_1 = 0.2$. This is a physically unacceptable small value since it implies a very large delocalization of the $3d^9$ hole. With $k_1 = 0.7$, Eq. (2) predicts $g_7 = 1.6$, which differs markedly from the experimental value. This discrepancy is considered as convincing evidence for the presence of a dynamic JT effect. With the parameters from Sec. III C, Eq. (3) accurately fits the observed g_7 value for a coupling strength $S = 1.5$. It has been shown²¹ that Eq. (3) slightly overestimates the JT quenching of g_7 . Therefore a somewhat larger S value, near 1.7, is more appropriate.

The 44-cm^{-1} sideband in the emission spectrum is

too low in energy to be interpreted as a simple unshifted lattice phonon. Neither can it be assigned to a totally symmetric impurity local mode, since such a mode would appear in both the emission and the absorption spectrum.²⁷ If the JT model suggested above is meaningful, it should also account for this line. The origin of shifted vibronic bands as a result of the JT coupling has been discussed in detail by Ham and Slack,²⁷ and examples for such bands occur in the crystal-field spectra of Fe²⁺,²⁷ Co²⁺,⁴⁶ Ni²⁺,⁴⁷ Cu²⁺ in ZnS,²⁰ and Ni²⁺ in GaP.^{9,47} In the present case, the numerical calculations of Clerjaud and Gelineau²¹ for ZnS:Cu²⁺ are of special relevance, since they directly apply to GaP:Ni⁺. From their Fig. 4 one infers (using $\lambda_1/\hbar\omega = -1.37$, $\hbar\omega = 3.50 \text{ cm}^{-1}$) that the first vibronic sideband for the $\Gamma_8^{(1)} \rightarrow \Gamma_7$ transition lies about 50 cm^{-1} above the ZPL if the JT coupling strength S is slightly less than two ($S \leq 2$). This estimate is almost identical with the value obtained from fitting g_7 , so that both results independently imply a JT energy between 600 and 660 cm^{-1} .

The JT model also offers an explanation for the failure to observe the $\Gamma_8^{(1)} \rightarrow \Gamma_8^{(2)}$ ZPL in luminescence near the energy ($\sim 4650 \text{ cm}^{-1}$) predicted by static crystal-field theory. The JT interaction mixes the vibronic $\Gamma_8^{(2)}$ ground state with excited vibronic Γ_8 levels of Γ_7 , thus transferring part of the $\Gamma_8^{(1)} \rightarrow \Gamma_8^{(2)}$ zero-phonon intensity into vibronic levels of Γ_7 , e.g., the 44-cm^{-1} sideband.

2. ²E excited state

It is evident that the experimental $\Gamma_8^{(1)}$ g values cannot be simultaneously fitted with Eqs. (6a) and (6b) irrespective of the value chosen for $k_2\lambda_2/\Delta$. On the other hand, the predicted g_1 value of 1.52 reasonably agrees with observation. This again is considered to be a manifestation of the JT coupling which leaves g_1 unchanged, but quenches g_2 according to Eq. (7). Both g_1 and qg_2 can be nicely reproduced ($g_1 = 1.52$, $qg_2 = -0.24$) if the JT reduction factor q is taken to be near its lower limit, $q \approx \frac{1}{2}$. Figure 2 of Ref. 24 then implies $S = E_{JT}/\hbar\omega \geq 1$, i.e., a moderate or even strong JT coupling with an E -type vibrational mode. However, the absorption spectrum in Fig. 5 evidently excludes the case of a strong JT coupling within the ²E state.

VI. CONCLUSION

This work demonstrates that nickel in GaP is not a simple deep acceptor but also acts as a two-electron trap in n -type material. The charge state corresponding to the doubly filled electron trap, Ni⁺($3d^9$), has been identified by an analysis of luminescence, absorption, Zeeman, and EPR spectra.

The ability of transition-metal impurities to act as deep two-electron traps in III-V compounds has only recently been recognized from EPR work on Cr in GaAs,^{2,3} and GaP,⁵ and on Fe in GaP.⁴ Now, this finding is also supported by electrical and optical^{48,49} measurements. One anticipates that such two-electron-trap states may deleteriously affect the minority carrier lifetime and diffusion length because of their twofold negative charge. For instance, minority holes injected into n -type material might be preferentially captured by such centers due to their strong Coulomb attraction. In fact, recent capacitance data⁵⁰ show that an efficient hole trap at $E_v + 0.95 \text{ eV}$ is associated with Ni in n -type GaP. It has been suggested⁵⁰ that this trap corresponds to a Ni_{Ga}-V_P complex. Whether this is correct or, whether the 0.95-eV trap is simply the isolated Ni⁺ center, must be clarified by further work. So far, from EPR there is no evidence for such a complex. In this connection it should also be mentioned that the degrading influence of Ni on the minority carrier properties of n -type GaAs has been recently revealed by a scanning electron-microscope technique.⁵¹

As far as its internal structure is concerned, the Ni⁺ center in GaP is the most completely characterized and best understood transition-metal center in a III-V compound. On the other hand, ionization and capture energies involving the Ni⁺ charge state are not yet known and the role of Ni as a luminescence killer in GaP light-emitting diodes must be elucidated by further experiments.

ACKNOWLEDGMENTS

We thank Dr. P. Koidl and Dr. O. F. Schirmer for a critical reading of the manuscript. The technical assistance of K. Daum, F. Friedrich, K. Langer, K. Sambeth, and M. Schlabach is gratefully acknowledged. We also thank Dr. J. Raab and Dr. C. Weyrich, Siemens AG, who supplied the GaP starting material. Part of this work has been supported by the technological program of the federal department of research and technology of the FR Germany.

¹R. W. Haisty and G. R. Cronin, in *Physics of Semiconductors, Proceedings of the 7th International Conference, Paris, 1964* (Academic, New York, 1964), p. 1161.

²U. Kaufmann and J. Schneider, *Solid State Commun.* **20**,

143 (1976).

³G. H. Stauss and J. J. Krebs, in *Proceedings of the Sixth International Symposium on GaAs and Related Compounds, Edinburgh, 1976*, (Institute of Physics and Physical Society,

- London, 1976), p. 84.
- ⁴U. Kaufmann and J. Schneider, *Solid State Commun.* **21**, 1073 (1977).
- ⁵U. Kaufmann and W. H. Koschel, *Phys. Rev. B* **17**, 2081 (1978).
- ⁶P. J. Dean, A. M. White, B. Hamilton, A. R. Peaker and R. M. Gibb, *J. Phys. D* **10**, 2545 (1977).
- ⁷S. A. Abagyan, G. A. Ivanov, and G. A. Koroleva, *Sov. Phys. Semicond.* **10**, 1056 (1976).
- ⁸U. Kaufmann and J. Schneider, *Solid State Commun.* **25**, 1113 (1978).
- ⁹J. M. Baranowski, J. W. Allen, and G. L. Pearson, *Phys. Rev.* **167**, 758 (1968).
- ¹⁰See, e.g., R. K. Watts, *Point Defects in Crystals* (Wiley, New York, 1977), Chaps. 8,9.
- ¹¹U. Kaufmann, *Phys. Rev. B* **11**, 2478 (1975).
- ¹²K. Leutwein, *Appl. Opt.* **10**, 46 (1971).
- ¹³G. F. Koster, J. O. Dimmock, R. G. Wheeler, and H. Statz, *Properties of the Thirty-Two Point Groups* (MIT, Cambridge, Mass., 1963).
- ¹⁴Orbital states are labelled according to Mulliken's notation. Spin-orbit states are classified according to the Γ notation of Ref. 13.
- ¹⁵A. Abragam and B. Bleaney, *Electron Paramagnetic Resonance of Transition Ions* (Clarendon, Oxford, 1970).
- ¹⁶M. Schulz and G. G. Wepfer, *Solid State Commun.* **10**, 405 (1972).
- ¹⁷R. K. Watts, *Phys. Rev.* **188**, 568 (1969).
- ¹⁸M. de Wit, *Phys. Rev.* **177**, 441 (1969).
- ¹⁹M. Wöhlecke, *J. Phys. C* **7**, 2557 (1974).
- ²⁰H. Maier and U. Scherz, *Phys. Status Solidi B* **62**, 153 (1974).
- ²¹B. Clerjaud and A. Gelineau, *Phys. Rev. B* **9**, 2832 (1974).
- ²²M. D. Sturge, in *Solid State Physics 20*, edited by F. Seitz and D. Turnbull (Academic, New York, 1967).
- ²³F. S. Ham, *Phys. Rev.* **138**, A1727 (1965).
- ²⁴F. S. Ham, *Phys. Rev.* **166**, 307 (1968).
- ²⁵J. T. Vallin, G. A. Slack, S. Roberts, and A. E. Hughes, *Phys. Rev. B* **2**, 4313 (1970).
- ²⁶J. T. Vallin and G. D. Watkins, *Phys. Rev. B* **9**, 2051 (1974).
- ²⁷F. S. Ham and G. A. Slack, *Phys. Rev. B* **4**, 777 (1971).
- ²⁸R. Parrot, C. Naud, C. Porte, D. Fournier, A. C. Boccara, and J. C. Rivoal, *Phys. Rev. B* **17**, 1057 (1978).
- ²⁹A. T. Vink and G. G. P. van Gorkom, *J. Lumin.* **5**, 379 (1972).
- ³⁰P. Koidl, *Phys. Status Solidi B* **14**, 477 (1976).
- ³¹B. Bleaney, *Proc. Phys. Soc. London, Sect. A* **73**, 939 (1959).
- ³²G. F. Koster and H. Statz, *Phys. Rev.* **113**, 445 (1959).
- ³³A. K. Bhattacharjee and S. Rodriguez, *Phys. Rev. B* **6**, 3836 (1972).
- ³⁴The energy scale of all optical spectra in this paper refers to vacuum wave numbers. This scale was calibrated against the energy of the sharp water-vapor absorption lines in the 5350-cm⁻¹ region as tabulated in Ref. 35.
- ³⁵H. H. Nielsen, *Phys. Rev.* **62**, 422 (1942).
- ³⁶R. M. Hoff and J. C. Irwin, *Can. J. Phys.* **51**, 63 (1973).
- ³⁷J. H. Haanstra and A. T. Vink, *J. Raman Spectr.* **1**, 109 (1973).
- ³⁸R. S. Title, *Phys. Rev.* **154**, 668 (1967).
- ³⁹R. Dingle, *Phys. Rev. Lett.* **23**, 579 (1969).
- ⁴⁰G. F. Imbusch, W. M. Yen, A. L. Schawlow, G. E. Devlin, and J. P. Remeika, *Phys. Rev.* **136**, A481 (1964).
- ⁴¹V. Heine and C. H. Henry, *Phys. Rev.* **11**, 3795 (1975).
- ⁴²U. Kaufmann (unpublished).
- ⁴³U. Kaufmann, P. Koidl, and O. F. Schirmer, *J. Phys. C* **6**, 310 (1973).
- ⁴⁴B. Clerjaud and A. Gelineau, *Phys. Rev. B* **16**, 82 (1977).
- ⁴⁵F. Mehran, T. N. Morgan, R. S. Title, and S. E. Blum, *J. Mag. Res.* **6**, 620 (1972).
- ⁴⁶P. Koidl, O. F. Schirmer, and U. Kaufmann, *Phys. Rev. B* **8**, 4926 (1973).
- ⁴⁷U. Kaufmann and P. Koidl, *J. Phys. C* **7**, 791 (1974).
- ⁴⁸M. R. Brozel, J. Butler, R. C. Newman, A. Ritson, D. J. Stirland, and C. Whitehead, *J. Phys. C* **11**, 1857 (1978).
- ⁴⁹T. Instone and L. Eaves, *J. Phys. C* **11**, L771 (1978).
- ⁵⁰B. Hamilton and A. R. Peaker, *Solid State Electron.* **21**, 1513 (1978).
- ⁵¹D. L. Partin, A. G. Milnes, and L. F. Vassamillet, *J. Electron. Mat.* **7**, 279 (1978).